Effects of Ca-Doping on the Vortex Properties and Pairing Symmetry of $(Y_{1-x}Ca_x)Ba_2Cu_3O_{7-\delta}$

Austin Moehle

Senior Thesis

Mentor: Prof. Nai-Chang Yeh

Motivations and Technical Background

The subject of this thesis is the high-temperature cuprate superconductor $(Y_{1-x}Ca_x)Ba_2Cu_3O_{7-\delta}$ (Ca-doped YBCO), whose structure is displayed in Figure 1.

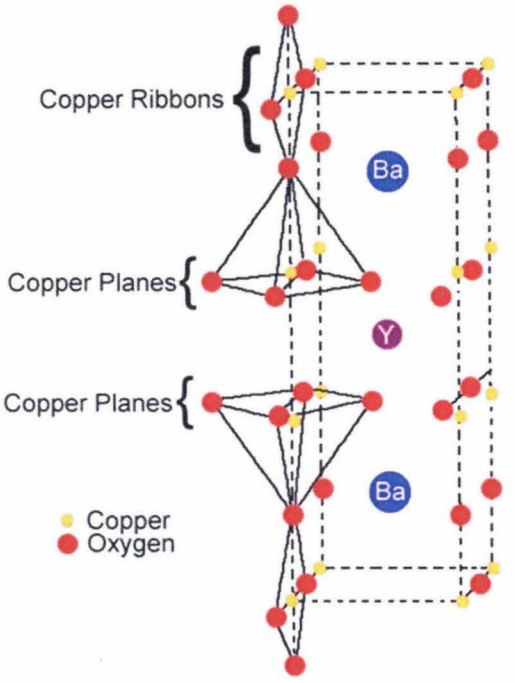

Figure 1 | YBCO structure with CuO_2 planes oriented horizontally.

Unlike type-I superconductors in a magnetic field (H) below the thermal dynamic critical field H_c, which have a single abrupt transition between the pure superconducting state that completely expels magnetic flux (also known as the Meissner phase) and the normal state, conventional type II superconductors can occupy an intermediate "vortex solid" phase between the upper critical field H_{c2} and the lower critical field H_{c1}, where superconductivity is partially lost due to the appearance of magnetic flux vortices throughout the material. In the case of extreme type-II superconductors such as the high-temperature cuprate superconductors, strong quantum/thermal/disorder fluctuation effects [1] result in a "vortex liquid" state below the upper critical field (Figure 2), in which vortices begin to drift around the sample as if they comprised a viscous liquid. This movement of vortices under an applied current creates electrical resistance in the material. For $H_{c1} < H < H_{c2}$, the temperature of transition between the vortex solid and vortex liquid phases occurs is known as $T_{irr}(H)$, the irreversibility temperature. The occurrence of strong fluctuation effects and a substantial region of the vortex liquid phase in the vortex phase diagram may be attributed to the weak superconducting stiffness in the cuprate superconductors as the result of coexisting competing orders (COs) and superconductivity [1].

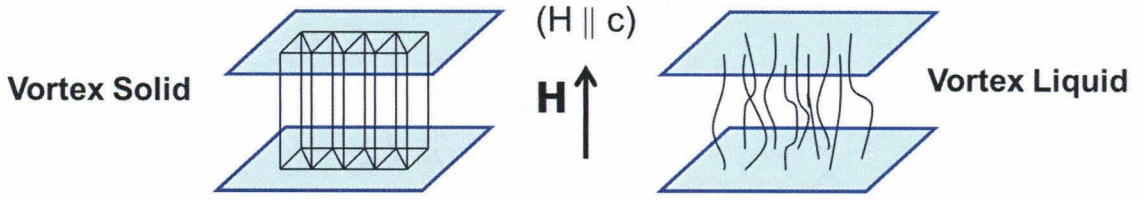

Figure 2 | Illustrations of the vortex solid and vortex liquid phases. (Images courtesy of Professor N.-C. Yeh)

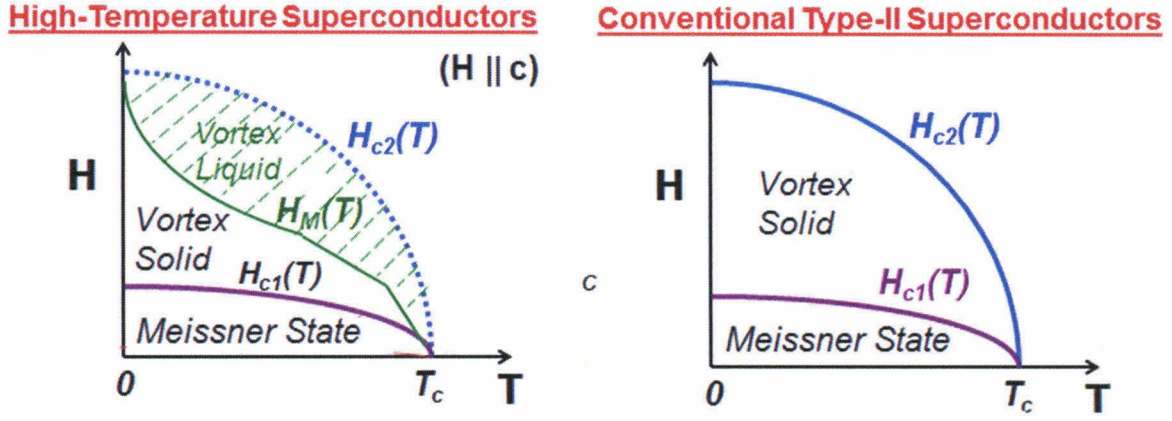

Figure 3 | Approximate phase diagrams of high-temperature and conventional type-II superconductors. (Images courtesy of Professor N.-C. Yeh)

In this paper we examine the effects of calcium doping on the vortex properties and pairing symmetry of YBCO. Epitaxial thin-film samples of Ca-doped YBCO at four different doping levels (x=0.05, 0.10, 0.125, 0.20) were grown by pulsed laser deposition (PLD) onto $(LaAlO_3)_{0.3}(Sr_2AlTaO_6)_{0.7}$ (LSAT) substrates and checked for quality by X-ray diffraction (XRD). In general calcium doping contributes excess holes to the CuO_2 planes, and in the hole-type cuprates such as the YBCO system, increasing hole concentration (p) beyond the optimal doping level can suppress the CO phase, as schematically shown in the temperature (T) vs. hole doping (p) phase diagram in Figure 4. Therefore, we predicted that increasing the hole doping level by controlling the calcium doping (x) and oxygen vacancies (δ) would reduce the competing order (CO) and favor the vortex-solid phase, causing an upward shift in the phase boundary $T_{irr}(H,x,p)$ between the vortex solid and vortex liquid phases (Fig. 5).

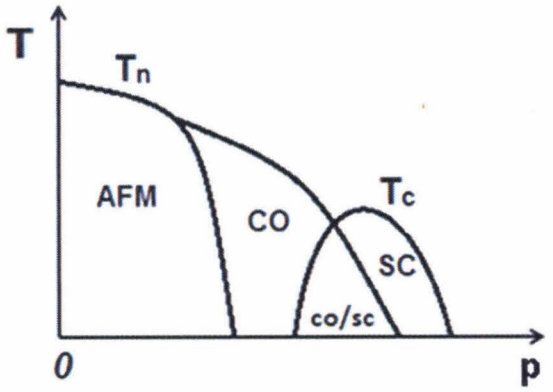

Figure 4 | YBCO phase diagram as a function of temperature (T) and hole-doping level (p), where AFM, CO and SC represent antiferromagnetism, competing order and superconductivity, respectively.

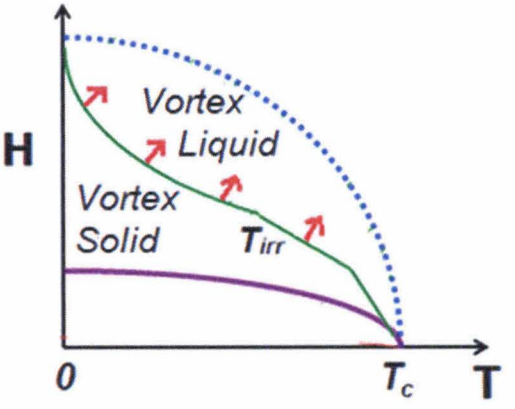

Figure 5 | Expected shift in irreversibility line with increasing hole-doping (p).

To test this hypothesis, the Ca-doped YBCO samples were subjected to magnetization measurements using a SQUID system to directly determine $T_c(H,x,p)$ and $T_{irr}(H,x,p)$, the superconducting transition and irreversibility temperatures, respectively, as a function of applied magnetic field (H), Ca doping level (x) and hole doping level (p). This data will allow for a systematic study of the effects of doping on the irreversibility line shown in Figure 5.

We also attempted to observe trends based on the pairing symmetry of Ca-doped YBCO. At zero or low Ca doping levels, the order parameter $\Delta_{sc}(\mathbf{k})$ has purely d-wave symmetry so that $\Delta_{sc}(\mathbf{k}) = \Delta_d\cos(2\theta_k)$ where θ_k is the angle between the momentum k and the antinodal direction of the pairing potential. However, as the doping level is raised, the order parameter also incorporates s-wave symmetry so that $\Delta_{sc}(\mathbf{k}) = \Delta_s + \Delta_d\cos(2\theta_k)$ [2]. This shift should manifest as characteristic energy gaps in c-axis tunneling conductance spectra obtained using a scanning tunneling microscopy (STM) system. We expect the contribution of the energy gap Δ_s relative to Δ_d to increase as the doping level is raised.

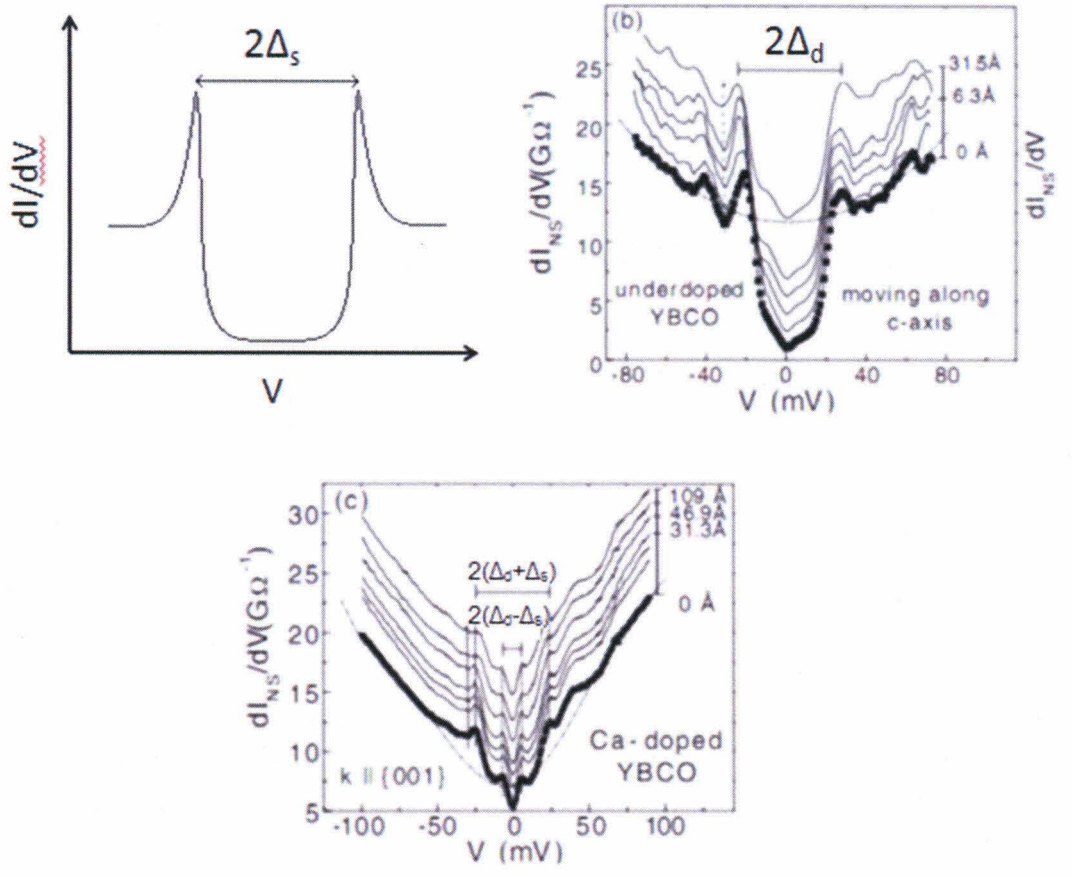

Figure 6 | Expected tunneling conductance spectra for (a) s-wave, (b) pure $d_{x^2-y^2}$-wave, and (c) ($d_{x^2-y^2}$+s)-wave systems with labeled energy gaps. (Figures 6(b) and 6(c) adapted from Ref. [2])

Sample Preparation

A schematic of the pulsed laser deposition (PLD) system is given in Figure 7. As illustrated in the figure, PLD utilizes a high power pulsed laser beam to vaporize material from the target in the form of a plasma plume. The apparatus is arranged such that the plume concentrates at the site of the substrate holder, allowing the material to be deposited as a thin film on the substrate surface. The growth conditions (such as the temperature of the substrate, the oxygen partial pressure in the vacuum chamber, the laser energy, the cooling rate after deposition, etc.) are very important and specific to the material to be deposited.

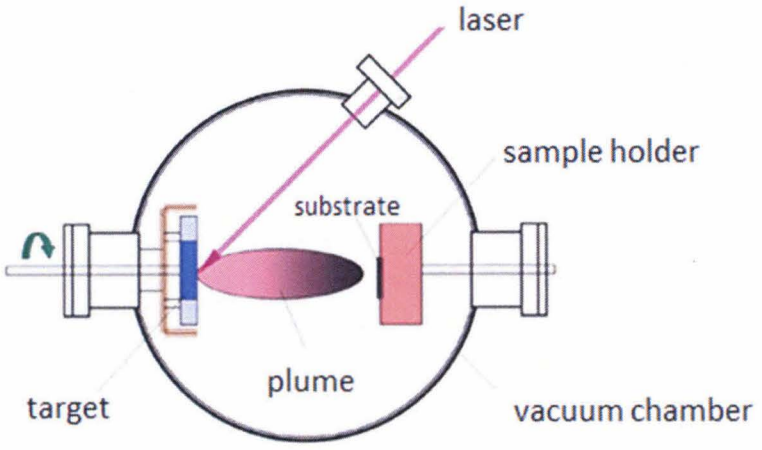

Figure 7 | Diagram of the pulsed laser deposition (PLD) system.

For this project, epitaxial thin films of $(Y_{1-x}Ca_x)Ba_2Cu_3O_{7-\delta}$ (YBCO) across a variety of calcium doping levels (x = 0.05, 0.10, 0.125, 0.2) were created by pulsed laser deposition (PLD) at 800-850 °C of pre-made Ca-doped YBCO polycrystalline targets onto $(LaAlO_3)_{0.3}(Sr_2AlTaO_6)_{0.7}$ (LSAT) substrates, using a laser energy of 300 mJ at 10 Hz with 50k pulses under an oxygen pressure of 384 mTorr. Following each deposition, each new sample was immediately annealed in oxygen, cooling from 960 °C to room temperature at a rate of 1 °C/min under oxygen pressure of 460 Torr. The films were a shiny black color, as expected for YBCO thin films, and appeared to be uniform and of sufficient quality.

These growth conditions were the result of extensive testing. To date, four batches of samples across the four doping levels (x = 0.05, 0.10, 0.125, 0.20) have been grown but only the latest batch has been determined to be of sufficient quality for study. Thin film quality was confirmed by X-ray diffraction and the superconducting transition temperature (T_c) determined by SQUID magnetization measurements.

Sample Quality Check

X-ray diffraction measurements using the standard θ-2θ method were used to confirm structural quality. A schematic of the X-ray diffraction apparatus is shown in Figure 8.

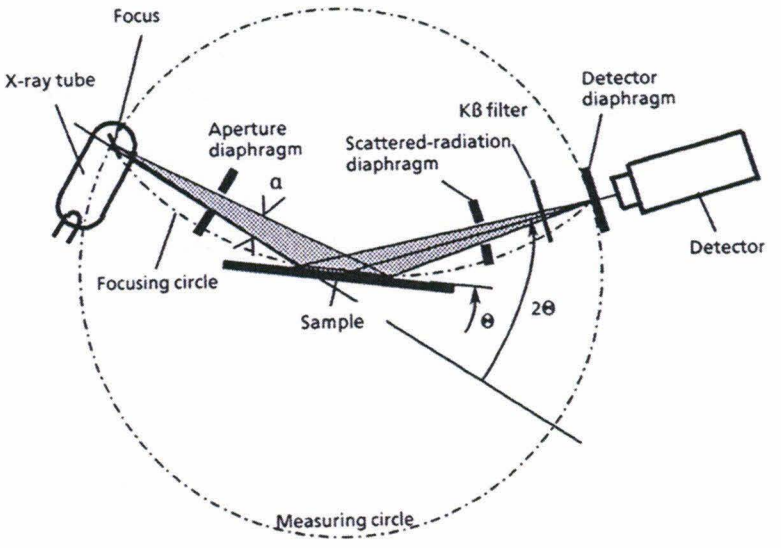

Figure 8 | Schematic of X-ray diffraction experiment. (Figure adapted from [6])

In the θ-2θ method, the X-ray source (in this case copper) is held fixed while the sample is rotated at a fixed rate and the detector is rotated at double that rate. With this setup the X-rays are diffracted at an angle 2θ from the initial beam and focused directly at the detector, allowing one to obtain spectra of detector intensity vs. 2θ. The diffraction spectra for x=0.05, 0.10, and 0.20 are stacked for comparison in Figure 9.

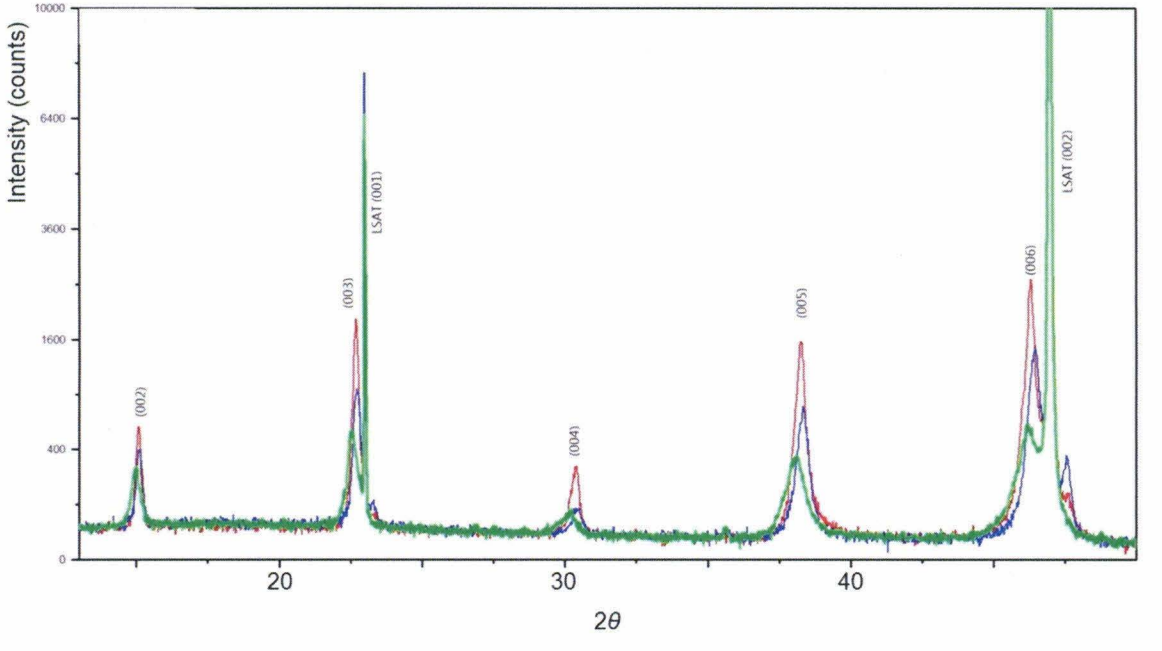

Figure 9 | X-ray diffraction data taken using the θ-2θ method. Red: x=0.05, Blue: x=0.10, Green: x=0.20. The peaks are labeled with the corresponding lattice planes.

From the 2θ peak values and the fact that the (00n) lattice planes are separated by a distance of d = c/n (with n being an integer), the c-axis lattice constants are easily determined from the formula $2d\sin(\theta) = \lambda_{Cu}$, where λ_{Cu} = 1.54184 Å is the wavelength of the X-rays generated by the copper source. The calculated c-axis lattice constants for doping levels x = 0.05, 0.1, and 0.2 are given in Table 1.

Ca-doping level (x)	c-axis lattice constant (Å)
0.05	11.76282178
0.1	11.73726755
0.2	11.81341348

Table 1 | c-axis lattice constants vs. Ca-doping level (x).

These lattice constants are consistent with the range reported in the literature [3].

SQUID Magnetization Measurements

Magnetization measurements were carried out using the magnetic properties measurement system (MPMS) in Beckman Institute. The key element in this apparatus is a superconducting quantum interference device (SQUID), which consists of a closed superconducting loop that contains a Josephson junction in the current path [6]. Due to the non-linear behavior of the Josephson junction and quantized state of the superconducting loop, a SQUID can resolve extremely fine changes in external magnetic fields while operating in large fields up to several Teslas. The MPMS system is comprised of a SQUID connected to superconducting detection coils that couple inductively to the sample, a superconducting magnetic shield surrounding the SQUID, and a superconducting magnet to generate large magnetic fields. When the sample is moved through the detection coils, the magnetic moment of the sample induces a current in the coils, which the SQUID converts to a voltage output. A diagram of the sample holder and surrounding elements in the MPMS system is shown in Figure 10.

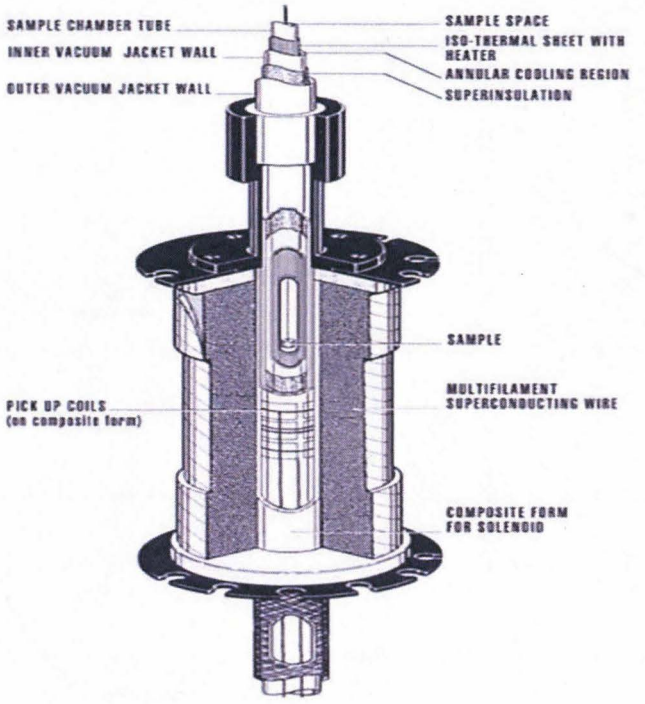

Figure 10 | Important components of the SQUID MPMS system. (Figure adapted from [6])

The MPMS system was used to measure magnetization vs. temperature by applying magnetic fields up to 5 Tesla parallel to the CuO_2 planes and measuring the resulting magnetization. For each measurement, the sample was cooled to 15 K in zero applied field, then a magnetic field applied and the sample slowly heated to above the superconducting transition temperature to obtain the zero-field-cool (ZFC) data. Next the sample was re-cooled to 15 K with the field still applied, then the sample slowly heated again in the presence of the field to obtain the field-cool (FC) data. Both the ZFC and FC data were used to compute the superconducting transition temperature (T_c) for each sample; this temperature was defined as the point at which the magnetization M began to deviate from its saturation value. These data were also used to compute the irreversibility temperature (T_{irr}), the temperature at which the ZFC and FC magnetization curves split from one another. The raw magnetization vs. temperature data under low applied field (H = 50 Oe) for all four samples are given below (Figure 11). The data displays several expected trends in the dependence of the superconducting transition temperature (T_c) and irreversibility temperature (T_{irr}) on the applied magnetic field (H) and calcium doping level (x).

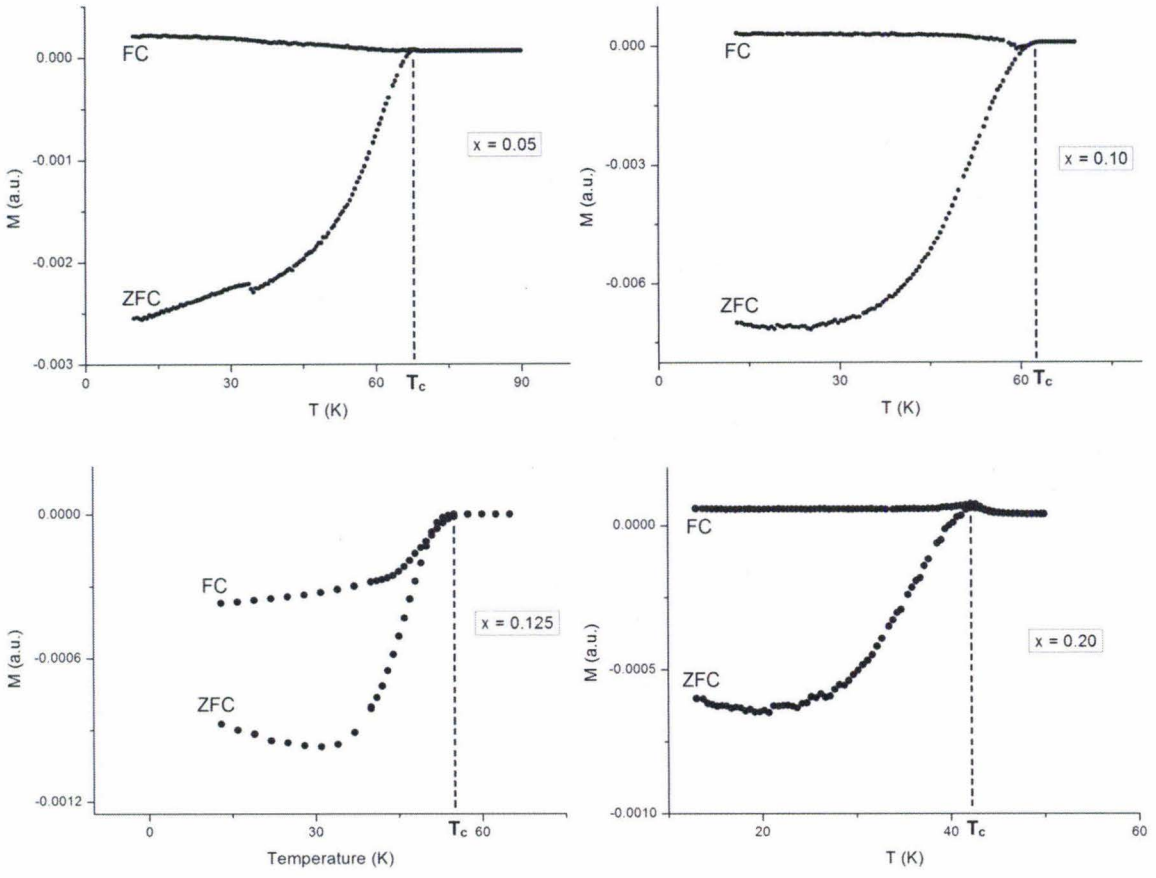

Figure 11 | FC and ZFC magnetization data under 50 Oe applied field for doping levels x = 0.05, 0.10, 0.125, 0.20.

Since zero magnetization indicates a complete expulsion of the magnetic field (a characteristic property of superconductors) we obtained the T_c values as the onset of zero magnetization. It is important to note that the hole doping level p for a given Ca-doping level x depends greatly on the oxygen annealing process [3], and that T_c can vary substantially for a given x as p is varied. The p value was calculated for each sample using empirically determined values of $T_{c,max}(x)$ [3], the maximum T_c value possible for a given x, and the empirical formula [4] $T_c(x,p) = T_{c,max}(x)$ [1-82.6(p-0.16)^2]. The results are given in Table 2. As expected, the T_c values drop monotonically as the Ca-doping level is increased.

x	0 [2]	0.05	0.10	0.125	0.20
T_c (K)	92.9	68	64	59	42
T_c^{max} (K)	93.5	91.2	89.0	87.5	82.9
p	0.15(2)	0.21(6)	0.21(8)	0.21(4)	0.23(8)

Table 2 | Values of T_c, T_c^{max}, and hole doping level p vs. Ca-doping level x.

FC and ZFC magnetization data were also obtained for higher applied fields up to 5 Tesla. While there are too many spectra to reasonably list here, two representative plots for x = 0.10 and 0.20 obtained using an applied field of 1 Tesla are given in Figure 12.

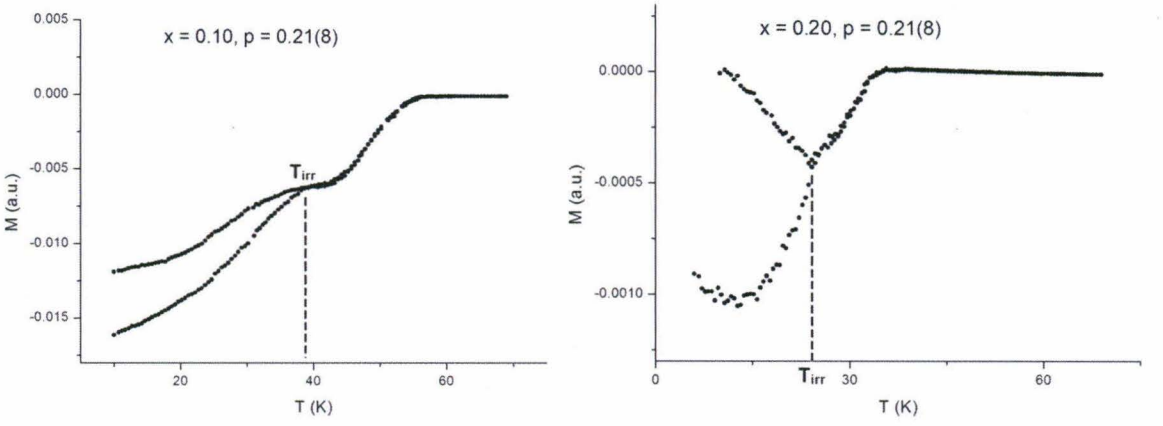

(a) (b)

Figure 12 | Representative plots of ZFC/FC data for high fields. T_{irr} is determined as the point of separation between the FC and ZFC curves. (a) x = 0.10, applied field H = 1 Tesla. (b) x = 0.20, applied field H = 1 Tesla.

From numerous plots similar to those shown in Figure 12, we determined the irreversibility temperatures T_{irr}(H) as the point of separation between the FC and ZFC curves. The resulting T_{irr} values were normalized to T_{c0}, the superconducting transition temperature under zero field, and the applied fields H normalized to $H_{c2} \sim 0.18T_c^2$ [5].

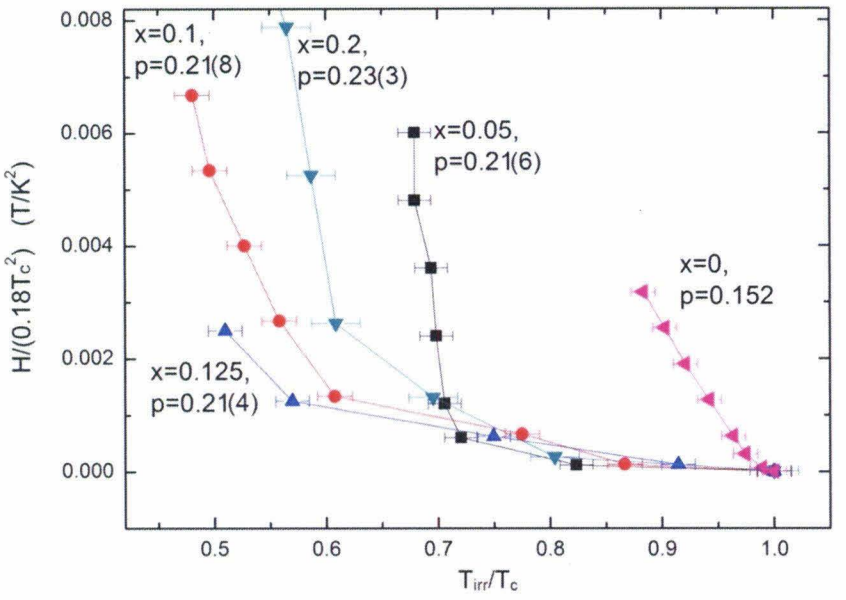

Figure 13 | Irreversibility lines (H vs. T_{irr}) for YBCO samples of varying Ca-doping (x) and hole-doping (p) values. Field values are normalized to $H_{c2} \sim 0.18T_c^2$ [5] and temperatures are normalized to T_{c0}.

As expected, the superconducting transition temperature (T_c) decreases as the calcium doping level is increased and the sample is overdoped. From Figure 13, we see that the normalized irreversibility line representing $T_{irr}(H,p,x)$ initially decreases with increasing Ca doping (x = 0.05, 0.10, 0.125) for approximately constant hole doping (p). This effect is likely due to suppression of superconductivity caused by Ca-induced disorder in the CuO_2 planes. As hole doping (p) increases further, this trend reverses and the irreversibility line increases; this is likely the result of vanishing competing orders (CO) favoring the vortex-solid phase, as originally suspected. Further investigation of these trends across a wider array of Ca doping and hole doping levels will be required to locate the point of reversal and fully determine the consistency of these trends.

STM Measurements

Cryogenic scanning tunneling spectroscopy was employed by other members in Professor Yeh's group to examine the dependence of the pairing symmetry in Ca-doped YBCO on the doping level. Spatially resolved tunneling conductance (dI/dV) vs. energy (ω = eV) spectra for the quasiparticle local density of states (LDOS) maps at T = 6 K were obtained for the x = 0.2 (p = 0.23) sample of Ca-doped YBCO prepared earlier. The data for this sample are given in Figure 14(a). From the energy gaps determined using the peak separations, we calculated the energy gaps Δ_d and Δ_s corresponding to the d-wave and s-wave contributions to the

superconducting pairing potential from the relations $\Delta_d + \Delta_s = \Delta_{SC}$ and $\Delta_{eff}^2 = \Delta_{SC}^2 + \Delta_{CO}^2$, along with a plot of Δ_{SC} and Δ_{CO} vs. p for zero field, which contains previously obtained data [2,5].

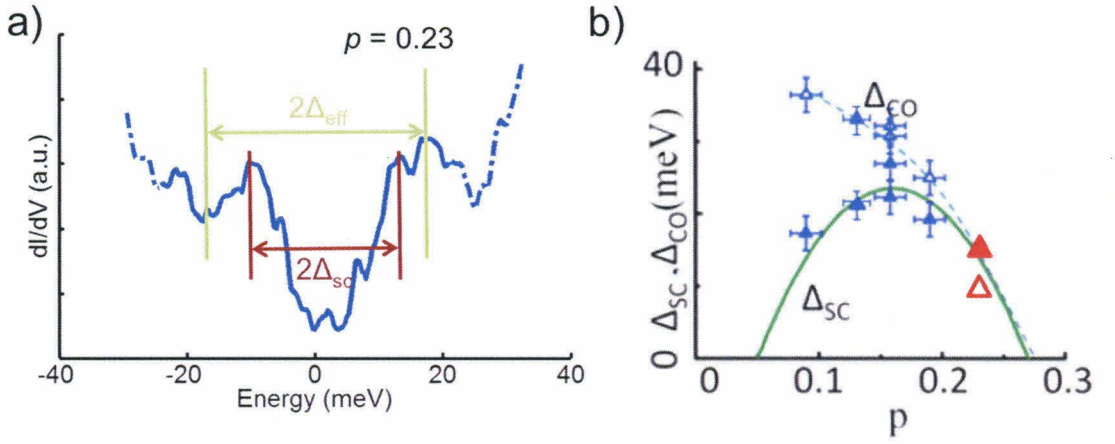

Figure 14 | (a) Tunneling conductance vs. energy spectra for the Ca-doped YBCO sample with x = 0.2 (p = 0.23) in zero field. Δ_d ~ 9 meV, Δ_s ~ 3 meV, Δ_{eff} ~ 16 meV, Δ_{SC} ~ 12 meV, Δ_{CO} ~10.5 meV. (Figure courtesy of Renee Wu). (b) Plot of Δ_{SC} and Δ_{CO} vs. p for zero field. The red triangles correspond to the Δ_{SC} (solid) and Δ_{CO} (outlined) values for the p = 0.23 sample under consideration. The Δ_{CO} value was obtained using the relation $\Delta_{eff}^2 = \Delta_{SC}^2 + \Delta_{CO}^2$. The blue triangles correspond to previously obtained data [2,5].

Interestingly, as indicated by the red triangles in Figure 14(b), p = 0.23 is the lowest doping level at which Δ_{CO} drops below Δ_{SC}. This is to be expected due to suppression of the competing order with increasing p. The data also reveals the effects of p on the relative contributions of Δ_d and Δ_s to the order parameter $\Delta_{SC}(k) = \Delta_d \cos(2\theta_k) + \Delta_s$, which are listed in the first two rows of Table 3 and in the plot of Δ_s/Δ_d vs. p in Figure 15. Both figures indicate that the s-wave contribution to the pairing potential increases as the hole doping level is increased beyond 0.15, which was the hypothesized trend.

p	0.09 [2]	0.15 [2]	0.19 [5]	0.23
Δ_d	20	29	16	9
Δ_s	0	0	3	3
Δ_{SC}	20	29	19	12
Δ_{CO}	36	32	27	10.5

Table 3 | Values of Δ_d, Δ_s, Δ_{SC}, and Δ_{CO} for various hole doping levels p. The first three columns of data are obtained from references [2,5].

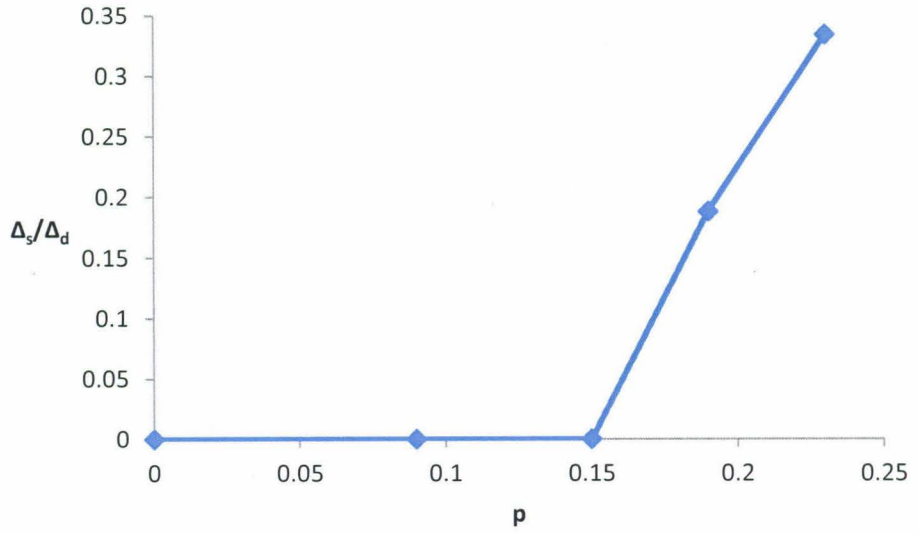

Figure 15 | Plot of Δ_s/Δ_d vs. p up to p = 0.23. The p = 0.23 sample was the subject of this section; the four leftmost data points were obtained from previous data [2,5].

Conclusions

Magnetization measurements on four Ca-doped YBCO samples (x = 0.05, 0.10, 0.125, 0.20) indicate that the irreversibility line $T_{irr}(H,x,p)$ initially drops when the Ca-doping level x is raised with hole doping p held constant. This effect is likely due to Ca-induced disorder. However, when p is raised from ~0.21 to ~0.23, the trend reverses, as we expected since increased hole doping reduces the competing order (CO) and increases the vortex-solid phase. STM measurements also reveal that raising the hole doping p above 0.15 causes an increase in the s-wave contribution to the superconducting pairing potential.

Acknowledgements

I would like to acknowledge Prof. Nai-Chang Yeh for serving as my mentor for this project and providing me with the opportunity to work with high-T_c superconductors. I also thank Prof. Zhenjie Feng who served as my guide on many experimental matters and provided invaluable help throughout the year. I acknowledge funding provided by NSF Grant #DMR0907251, by the Institute for Quantum Information and Matter, an NSF Physics Frontiers Center with support of the Gordon and Betty Moore Foundation, and by the Kavli Nanoscience Institute with support of the Kavli Foundation.

References

1. Yeh, N.-C., Beyer, A.D.: Int. J. Mod. Phys. B **23**, 4543 (2009)
2. Yeh, N.-C., et al.: Phys. Rev. Lett. **87**, 087003 (2001)
3. Fisher, B., et al.: Phys. Rev. B **47**, 6054 (1993)
4. Presland, M.R., et al.: Physica C **176**, 95 (1991)
5. Yeh, N.-C., Teague, M.L., Wu, R. T.-P., Feng, Z. J., Chu, H., Moehle, A. M. "Scanning Tunneling Spectroscopic Studies of the Low-Energy Quasiparticle Excitations in Cuprate Superconductors" Submitted to Proceedings of ICSM2012, Istanbul (April 29 – May 4)
6. McElfresh, M. "Fundamentals of Magnetism and the MPMS Instrument" http://mmrc.caltech.edu/MPMS/Fund_Mag_and_Mag_Meas.pdf